

# Diffusion of finite-size particles in channels with random walls

Maximilian Bauer,<sup>1,2</sup> Aljaž Godec,<sup>1,3</sup> and Ralf Metzler<sup>1,4,\*</sup>

<sup>1</sup>*Institute of Physics and Astronomy, University of Potsdam, D-14476 Potsdam-Golm, Germany*

<sup>2</sup>*Physics Department, Technical University of Munich, Garching, Germany*

<sup>3</sup>*National Institute of Chemistry, Ljubljana, Slovenia*

<sup>4</sup>*Physics Department, Tampere University of Technology, FI-33101 Tampere, Finland*

Diffusion of chemicals or tracer molecules through complex systems containing irregularly shaped channels is important in many applications. Most theoretical studies based on the famed Fick-Jacobs equation focus on the idealised case of infinitely small particles and reflecting boundaries. In this study we use numerical simulations to consider the transport of *finite-sized* particles through asymmetrical two-dimensional channels. Additionally, we examine *transient binding* of the molecules to the channel walls by applying sticky boundary conditions. With the application of diffusing pathogens in hydrogels in mind, we consider an ensemble of particles diffusing in independent channels, which are characterised by common structural parameters. We compare our results for the long-time effective diffusion coefficient with a recent theoretical formula obtained by Dagdug and Pineda [*J. Chem. Phys.*, 2012, **137**, 024107].

## I. INTRODUCTION

Civil aviation traffic has been broadly democratised within the last few decades, leading to ever-increasing numbers of both business and pleasure passengers. The downside of this increased worldwide connectivity is the very rapid global spreading of diseases [1]. Simultaneously, new infectious diseases are emerging, driven by human or ecologic causes [2], and microorganisms are developing various forms of multiple drug resistance [3, 4]. It is therefore imperative to develop more rapid, mobile, and reliable methods for pathogen detection. One of the paths being followed is the development of smart hydrogels, which respond to various stimuli [5–8].

The scenario we have in mind is that viral pathogens diffuse into the hydrogel, where they bind to specific sites and effect a local mechanical deformation. To cause macroscopic effects, the pathogens' size must be comparable to the typical mesh size of the hydrogel. A similar situation was investigated in a single particle tracking study of submicron tracer beads in reconstituted F-actin networks, observing *anomalous diffusion* [9]

$$\langle \mathbf{r}^2(t) \rangle \simeq t^\alpha, \quad (1)$$

where the anomalous diffusion exponent  $\alpha$  depended on the ratio of the tracer bead size versus the typical mesh size of the actin network: for relatively large beads  $\alpha$  was shown to decrease to zero, while for small beads  $\alpha$  converged to one, the case of normal diffusion [9]. Subdiffusion of the type (1) was observed for similarly-sized tracer beads in wormlike micellar solutions [10], as well as for the motion of various objects in the macromolecularly crowded cytoplasm of living cells such as the infectious pathway of adeno-associated viruses in living HeLa cells [11], as well as for submicron lipid and insulin granules

in living fission yeast and MIN6 insulinoma cells [12, 13]. For reviews on anomalous diffusion, see Refs. [14, 15], and for subdiffusion in crowded systems, see Refs. [16–18].

Given these experimental findings it is pertinent to ask whether the motion of pathogens in a hydrogel is equally subdiffusive. Here we address this question by considering the path of the pathogen through the hydrogel as the motion of a particle of finite size through a tortuous, corrugated channel with varying width. The particle gets repeatedly held up by bottlenecks in the channel, and may transiently bind to the channel walls, representing the interaction with specific binding site for the pathogen in the hydrogel. Using an ensemble of channel geometries in our numerical analysis, we account for the different paths the pathogen can take through the hydrogel. We find that indeed the particle in their channel performs transient subdiffusion, that we analyse in terms of the anomalous diffusion exponent, the number of successful moves with respect to the number of simulation steps, and the effective long-time diffusivity, as function of the characteristic channel geometry parameters.

The theoretical description of the motion of particles in confined geometries like channels (2D) or pores (3D) with varying width has a long-standing history (see [19] and references therein). In a seminal work Zwanzig derived a modified Fick-Jacobs equation which is at the basis of most subsequent quasi-one-dimensional descriptions [20],

$$\frac{\partial G(x, t)}{\partial t} = \frac{\partial}{\partial x} D(x) w(x) \frac{\partial}{\partial x} \frac{G(x, t)}{w(x)} \quad (2)$$

Here  $G(x, t)$  describes the local concentration of particles at position  $x$  and time  $t$ ,  $w(x)$  the width of the channel at position  $x$  and most importantly  $D(x)$  is an effective position-dependent diffusion coefficient. Subsequently, several different forms for  $D(x)$  were derived and applied to various systems [20–30]. Taking along only first order derivatives of the width profile  $w(x)$ , Kalinay and Percus [24] (see also Martens et al. [27]) obtained the closed

---

\*Electronic address: rmetzler@uni-potsdam.de

form result

$$D_{KP}(x) = D_0 \frac{\arctan(w'(x)/2)}{w'(x)/2}, \quad (3)$$

where  $D_0$  denotes the position-independent diffusion coefficient in the absence of confinement. We note that the presence of an  $x$ -dependent diffusivity in free space is sufficient to effect various forms of anomalous diffusion [31–33].

However, the above forms of  $D(x)$  are restricted to symmetric channels, i.e., channels with a straight centre-line. This constraint was removed in an approach by Bradley [35], which was subsequently generalised by Dagdag and Pineda to [36]

$$D_{DP}(x) = D_0 \left( \frac{\arctan\left(y'_0(x) + \frac{w'(x)}{2}\right)}{w'(x)} - \frac{\arctan\left(y'_0(x) - \frac{w'(x)}{2}\right)}{w'(x)} \right), \quad (4)$$

where  $y_0(x)$  denotes the vertical position of the centre-line at horizontal position  $x$ . Note that Eq. (4) generalises all the previous results for  $D(x)$ , for instance, one obtains the result (3) for symmetrical channels by setting  $y'_0(x) = 0$  [36].

As detailed by Zwanzig [20], in a system with periodic boundary conditions the effective diffusion coefficient in the long-time regime,  $D_{\text{eff}}$ , is obtained by using the following formula introduced by Lifson and Jackson [37] and generalised by Festa and Galleani d'Agliano [38],

$$\frac{1}{D_{\text{eff}}} = \left\langle \frac{1}{D(x)w(x)} \right\rangle \langle w(x) \rangle, \quad (5)$$

where  $\langle \cdot \rangle$  denotes the average over one period. Thus, for any channel with width profile  $w(x)$  and centre-line  $y_0(x)$ , Eq. (4) can be used to calculate  $D_{DP}(x)$ , which in turn is used in Eq. (5) to calculate the effective diffusion coefficient  $D_{\text{eff,DP}}$ .

The above theories based on the Fick-Jacobs formalism apply to point-like particles, that is, the particle can move along the channel as long as the width is not equal to zero. For our scenario of pathogens moving in a channel, we argued that the pathogen size is comparable to the channel width. Thus, the pathogen can only fully cross the channel when the width profile  $w(x)$  at any position is larger than the particle size. Systems containing finite-size particles were indeed studied in literature [39, 40]. Essentially, in all formulae the channel width  $w(x)$  has to be replaced by an effective channel width.

Another modification with respect to the Fick-Jacobs approach that we consider here concerns the boundary conditions. Usually, reflecting boundary conditions are used, i.e., when the particle collides with the channel walls, its perpendicular motion is simply reversed. In

the pathogen-hydrogel scenario, the pathogen will (transiently) bind to specific binding sites incorporated into the hydrogel. Here we explicitly include such effects by reactive boundary conditions, due to which the model particle will transiently be immobilised by binding to the channel wall. Moreover, it may immediately rebound to the channel wall after unbinding. As we will see, this has a major effect on the particle motion.

Finally, the conventional Fick-Jacobs approach describes the motion of particles in a single channel with quenched geometry. However, for the application to the pathogen motion in the hydrogel, we mimic the possibility for particles to move on different paths across the hydrogel by sampling an ensemble of tracer particles in an ensemble of channel geometries. This ensemble of channels is characterised by a common set of structural parameters.

The present study therefore represents an application of the Fick-Jacobs approach to the biophysical problem of pathogen motion in a complex, confining environment. At the same time, however, it significantly generalises the Fick-Jacobs model. The paper is structured as follows. In the subsequent section we introduce the details of the numerical approach used in this study. In section 3 we discuss how the numerical results are analysed in terms of time and ensemble averaged observables. In section 4 we present the detailed results. Section 5 puts our findings in perspective with respect to theory by Dagdag and Pineda, before drawing our conclusions in section 6.

## II. SIMULATION DETAILS

We study the diffusion through a two-dimensional channel with periodic boundary conditions in horizontal  $x$ -direction. In vertical  $y$ -direction the system is limited by two walls, see Fig. 1. These two walls are described by  $N$  points connected by straight lines, represented by the blue lines in Fig. 1. For numerical convenience the points of the channel wall reside on a lattice with unit lattice constant, which effectively determines the fundamental length scale of the system. Due to the horizontal periodic boundary conditions the two leftmost and the two rightmost wall points are identical. Their vertical distance (in  $y$ -direction) is denoted by  $g$ , see Fig. 1. This is one of the fundamental parameters of the system and is called gap opening parameter in the following.

We only consider channel configurations without touching or overlapping wall. Moreover, we solely allow wall configurations in which the  $y$ -coordinates of nearest neighbour points within one wall differ by at most unity. This excludes the occurrence of extremely rugged walls. Thus the size of the system is fully described by the gap opening parameter  $g$  and the two ‘displacement vectors’ of size  $(N - 1) \times 1$  for the upper and lower walls. The  $i^{\text{th}}$  entry of this displacement vector denotes the difference between the  $y$ -coordinate of the  $(i + 1)^{\text{st}}$  and  $i^{\text{th}}$  wall points for each of the two walls ( $i$  is counted from left

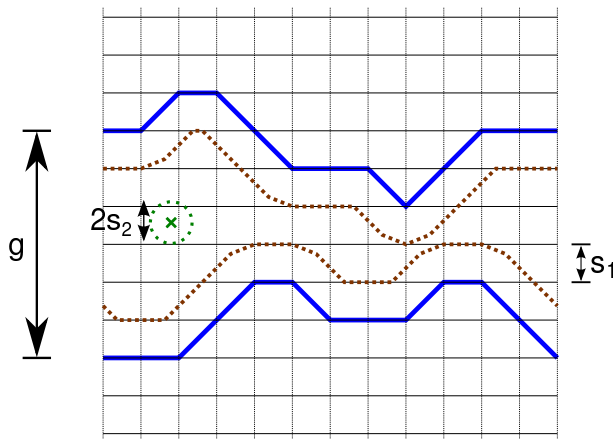


FIG. 1: Schematic of the channel with periodic boundary conditions. The blue lines depict the channel walls, while the dotted (brown) lines mark the excluded volume for a finite-sized particle. Parameters: gap opening  $g = 6$ , particle size  $s_1 = 1$ , step size  $s_2 = 0.6$ , ruggedness parameter  $M_1 = 6$ , and lateral channel length  $N = 12$ .

to right). Due to the constraints mentioned above only  $0, \pm 1$  are valid entries, and the sum of all entries per wall must be zero to fulfil the periodic boundary requirement.

We consider channel walls with different contour lengths. The parameter  $M_1$  describes the number of displacements of size  $\pm 1$  which occur in a wall. We thus call it the ‘ruggedness parameter’. Due to the periodic boundary constraint the number of jumps directed upwards must be equal to the one for jumps downwards for both walls. Consequently,  $M_1$  is an even number and lies in the interval  $[0, N - 1]$  (for odd  $N$ ) or  $[0, N - 2]$  (for even  $N$ ). We only consider configurations in which  $M_1$  is equal for the upper and lower walls. However, this does not confine our study to symmetric channels, compare Fig. 1.

The position of the random walking particle is described by the position of its centre of mass, illustrated by the green cross in Fig. 1. Its motion is off-lattice. This is shown in Fig. 1, where a circle of radius  $s_2$  (the step size of the random walk) is drawn around the particle’s current position. For each step a random angle with respect to the  $x$ -axis is drawn, and the particle attempts to move its centre to the corresponding point on the dotted circle. To account for the diffusion of finite-sized particles through the channel, before executing a step we check whether the distance from the current position to the wall is sufficient. To this end, the minimal distance to the wall is calculated for the trial position. Only if it is larger than the particle size  $s_1$ , the step is actually performed. This accessible space is limited by the two dotted brown lines in Fig. 1. Their vertical distance is the effective channel width for the finite-sized particle, and it is the quantity to be inserted into Eqs. (4) to (5). If the particle aims to move at a forbidden position, the step is cancelled and the particle remains at its current

position, but time is increased by one unit. This corresponds to ‘sticky’ boundary conditions, which mimic transient binding to the channel wall.

The diffusing particle is initially placed in the middle of the channel in both  $x$  and  $y$  directions. However, if such a starting position is not possible in the sense described above, the given channel configuration is dismissed and a new one chosen.  $T_{\max}$  random walk steps are performed and the position in the  $x$  direction is traced and analysed. If not stated otherwise, for each parameter set  $g$  and  $M_1$  the results were averaged over 25,000 configurations using the parameters  $N = 100$ ,  $T_{\max} = 10^6$ ,  $s_1 = 1$ , and  $s_2 = 0.6$ .

### III. EVALUATION PROCEDURE

A quantity of central interest when tracking the motion of single particles is the time-averaged mean squared displacement (TA MSD)

$$\overline{\delta_i^2(t)} = \frac{1}{T_{\max} - t} \int_0^{T_{\max} - t} dt' [x_i(t' + t) - x_i(t')]^2 \quad (6)$$

for the  $i^{\text{th}}$  time series  $x_i(t)$  along the horizontal direction. We use the fixed simulation time  $T_{\max}$ , and in what follows the bar denotes a time average. The TA MSD was subsequently averaged over all configurations to obtain the ensemble *and* time averaged mean squared displacement (EATA MSD)

$$\langle \overline{\delta^2(t)} \rangle = \frac{1}{N_{\text{conf}}} \sum_{i=1}^{N_{\text{conf}}} \overline{\delta_i^2(t)}. \quad (7)$$

Thus, the usual ensemble-averaged MSD is nothing but a special case of the ensemble- and time-averaged MSD, where the point of reference is the starting position. We also consider the ensemble averaged mean squared displacement (EA MSD) in  $x$ -direction,

$$\langle x^2(t) \rangle = \frac{1}{N_{\text{conf}}} \sum_{i=1}^{N_{\text{conf}}} [x_i(t) - x_i(0)]^2, \quad (8)$$

where  $N_{\text{conf}}$  denotes the number of different configurations, in our case  $N_{\text{conf}} = 25,000$ . Here and in the following  $\langle \cdot \rangle$  denotes the ensemble average over channel realisations.

As transient anomalous diffusion behaviour is not readily discernable in a conventional log-log plot of the MSD versus time, we visualise the data in terms of the MSD divided by time, as function of the logarithm of time, see Refs. [41, 42]. This method emphasises deviations from normal diffusion behaviour: curves with a negative slope represent subdiffusion. A typical plot is shown in Fig. 2. We observe a weaker form of subdiffusion for times from roughly 10 to  $10^3$  time steps. Around  $10^3$

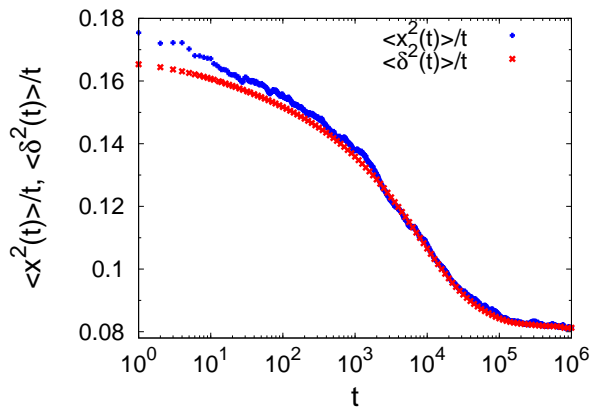


FIG. 2: Transient subdiffusion in an ensemble with gap opening parameter  $g = 6$  and wall ruggedness parameter  $M_1 = 30$ . We plot  $\langle x^2 \rangle / t$  (blue symbols) and  $\langle \delta^2 \rangle / t$  (red symbols) as function of time  $t$ . Note the logarithmic abscissa.

time steps, there is a turnover to a more pronounced subdiffusive behaviour. This regime persists until some  $10^5$  time steps, when the terminal normal diffusive appears. We note that both time and ensemble MSD coincide at longer times. On short time scales the EA MSD curve lies above the EATA MSD curve due to the fact that, by construction, at the beginning of each trajectory the particle is placed in the middle of the channel. At such short times the probability that the particle sticks to the wall is greatly reduced compared to later times, and thus the EA MSD attains larger values than the EATA MSD, which averages the behaviour along the entire time series. The anomalous behaviour displayed in Fig. 2 is one of the major results of this study.

In the following we study the slowing-down of the particle diffusion in terms of two quantities. First, in the normal diffusive behaviour beyond  $10^5$  time steps we fit the EATA MSD data with a linear function in order to obtain the effective long time diffusion coefficient  $D_{\text{eff}}$ . This quantity is then compared with the theoretical value  $D_{\text{eff,DP}}$  given by Eq. (5), since for each channel configuration we calculate  $D_{\text{DP}}(x)$  via Dagdug and Pineda's formula (4), where  $w(x)$  is replaced by the effective channel width. We normalise the value of the effective long time diffusivity by the corresponding value in absence of walls,  $D_{\text{rel}} = D_{\text{eff}}/D_0$ . Second, we obtain the anomalous diffusion exponent  $\alpha$  on time scales ranging from  $10^3$  to  $10^5$  time steps. Similar results are obtained by studying the mean maximal excursion of the particle [43] (data not shown).

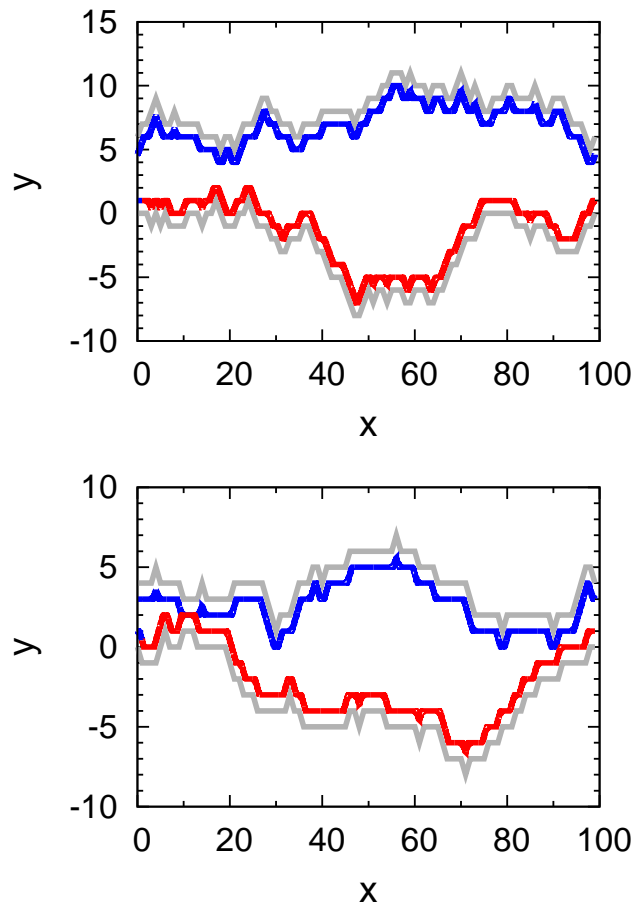


FIG. 3: Channel wall configurations characterised by the gap opening parameter  $g = 6$  and the wall ruggedness parameter  $M_1 = 50$  (upper panel) and  $g = 4$ ,  $M_1 = 30$  (lower panel). The actual upper and lower walls are plotted as grey lines. The region bounded by the red and blue curves are inaccessible for the particle.

## IV. RESULTS

### A. Fixed channel wall configuration

Before studying the effect of different parameter sets  $g$  and  $M_1$  to characterise the diffusion through this class of corrugated channels, we investigate in detail the features seen in Fig. 2 from simulations with fixed channel wall configurations.

We explicitly consider three exemplary configurations to illustrate the effect of the sticky boundary conditions. These configurations are characterised by the parameter pairs  $g = 6$  and  $M_1 = 0$ ,  $g = 4$  and  $M_1 = 30$ , and  $g = 6$  and  $M_1 = 50$ . The two configurations with non-flat walls are shown in Fig. 3. The grey curves denote the actual position of the channel walls, while the bold blue and red curves mark the region, which is inaccessible for the particle's centre.

While for a given wall configuration by the choice of

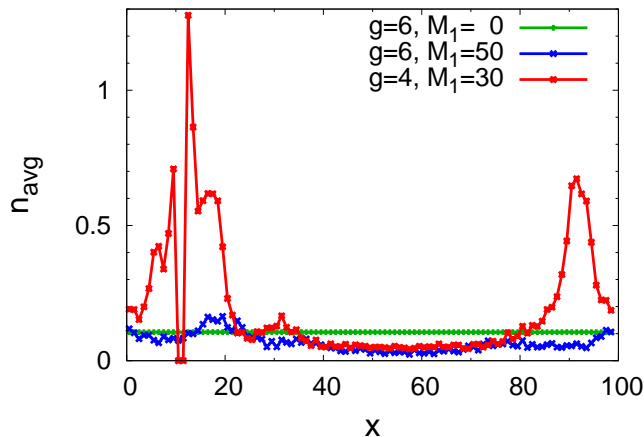


FIG. 4: Mean number  $n_{\text{avg}}$  of unsuccessful attempts to move to the next position along the channel as a function of the position  $x$  along the channel, for the three wall configurations characterised by  $g = 6$  and  $M_1 = 0$  (green line),  $g = 6$  and  $M_1 = 50$  (blue line), and  $g = 4$  and  $M_1 = 30$  (red line).

the gap opening parameter  $g$  we make sure that the particle finds sufficient space in the middle of the channel where it is initially placed, it is a priori not certain that the particle can traverse the entire channel. This is the case when at some point the upper and lower walls overlap. Strictly speaking, however, a passage is impossible only if there exists an overlap area whose width is at last of the step size  $s_2$ . Otherwise, due to the finite step size the particle can actually ‘tunnel’ through such bottlenecks. The wall configuration depicted in the upper panel of Fig. 3 does not allow such a tunnelling for the given parameters  $g = 6$  and  $M_1 = 50$ : the red and the black curve do not overlap. The situation is different in the lower panel of Fig. 3 with  $g = 4$  and  $M_1 = 30$ : the channel is blocked for the particle at  $x \approx 12$ .

However, even if inaccessible regions in a given wall configuration exist but the overlap of the walls stretches over less than the distance  $2 \times s_2$ , such a narrow straight constitutes a severe entropic bottleneck for the diffusing particle: there exists an appreciable possibility that the particle repeatedly sticks to the channel walls. To quantify the influence of the sticky walls we binned the channels into 99 cells of length 1 and extracted from our simulations how often the particle unsuccessfully tries to move to a new position while being in the corresponding bin.

We first study the mean number  $n_{\text{avg}}$  of unsuccessful attempts for the three above sample configurations as a function of the particle position along the channel in Fig. 4. The green curve for the parameters  $g = 6$  and  $M_1 = 0$  shows that for flat walls  $n_{\text{avg}}$  is approximately constant. The fact that this value is finite is a consequence of the sticky boundary condition at the edges of the system: namely, move attempts which would end at a position which is forbidden due to the finite size of the

particle are not executed. If reflective walls were considered, any step could be executed and then  $n_{\text{avg}} = 0$ . In the present case, the value of  $n_{\text{avg}}$  depends on the step size and the (constant) width of the channel. From Fig. 4 we deduce that  $n_{\text{avg}} \approx 0.1056$ .

The blue curve in Fig. 4 for  $g = 6$  and  $M_1 = 50$  shows some variation as function of  $x$ : where the channel is narrow, e.g., around  $x \approx 20$  in the upper panel of Fig. 3,  $n_{\text{avg}}$  is much higher than at locations where the channel is wider, e.g., in the middle of the channel. Comparing the minimum and maximum of  $n_{\text{avg}}$  along the channel, the variation of  $n_{\text{avg}}$  makes up a factor of approximately 7. This effect is much more pronounced in the red curve in Fig. 4 for the parameters  $g = 4$  and  $M_1 = 30$ , corresponding to the lower panel of Fig. 3: the curve is broken as two bins of the channel are inaccessible for the particle. In the bin to the right of the channel blockage the average number of unsuccessful tries is larger than 1. In other regions of the channel  $n_{\text{avg}}$  attains values similar to the ones in the other two configurations. Hence, the mean number of unsuccessful motion attempts along the channel directly reflects the effective channel width and thus the local transport properties.

Additional information can be deduced from studying the probability distribution  $p(n_{\text{uns}})$  of the number  $n_{\text{uns}}$  of unsuccessful attempts in a row shown in Fig. 5, where we focus on the most distinct configuration with parameters  $g = 4$  and  $M_1 = 50$  corresponding to the lower panel of Fig. 3. For better visibility we only consider extreme cases: namely, only the two bins with the highest and the two bins with the lowest mean number of motion attempts. In all four cases, the probability to find higher values of  $n_{\text{uns}}$  decreases. In regions where the channel is wide (green and blue symbols in Fig. 5) this decay is very fast, such that within our simulation time there were never more than 19 subsequent unsuccessful attempts. Otherwise, it becomes obvious that near severe bottlenecks the distribution of waiting times is much more heavy-tailed (black and red symbols in Fig. 5). Up to 100 unsuccessful attempts in a row are possible, with a probability of about  $10^{-6}$ .

With this information, let us go back to the features of Fig. 2. According to the Fick-Jacobs theory, whenever the width of the channel changes in the form of a bottleneck or a bulge, this slows down the diffusion of the particle [20]: in the case of a bottleneck the particle may be reflected back, while in the case of a bulge the particle may execute many motion events off the minimal path along the channel. The effect of the entropic bottlenecks in our present case is amplified by the presence of the sticky boundary conditions. On all time-scales on which the particle interacts with the walls, it is slowed down in comparison to a particle moving in free space. This induces the transient subdiffusion in the ensemble and time averaged trajectories. On very long time scales, when the configurations shown in Fig. 3 are equivalent to a single step size in a coarse-grained random walk on the whole periodic structure, normal diffusive behaviour is restored,

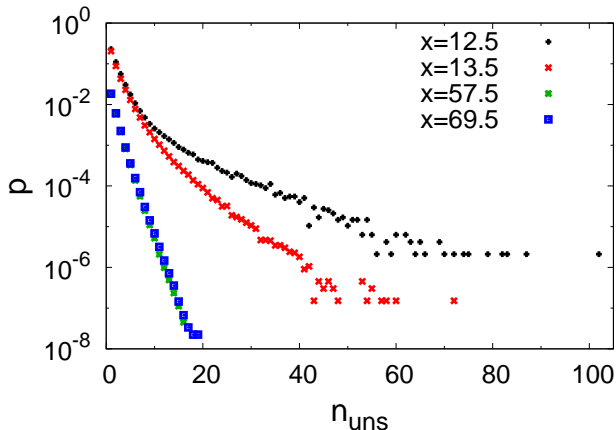


FIG. 5: Probability distribution for the number of subsequent unsuccessful motion attempts,  $n_{\text{uns}}$ , obtained with the wall configuration corresponding to the lower panel of Fig. 3 with parameters  $g = 4$  and  $M_1 = 30$ . We show the statistics for the bins centred around:  $x = 12.5$  (black symbols),  $x = 13.5$  (red symbols),  $x = 57.5$  (green symbols), and  $x = 69.5$  (blue symbols). The symbols for  $x = 57.5$  are almost fully covered by those for  $x = 69.5$ .

but now with a reduced diffusion coefficient. This reduced coefficient takes into account all the intermediate contacts with the channel walls. Thus, it is expected that more corrugated and/or tighter channels, which imply more frequent interaction with the walls should show reduced values of  $\alpha$  and a reduced effective diffusion coefficient on the ensemble level. To study these effects, in the following we systematically study the impact of the parameters  $g$  and  $M_1$  on the transport through the channels in ensembles of size 25,000.

### B. Simulations of channel ensembles

Two main simulations series were performed with the fixed values  $g = 6$  and  $g = 4$  for the gap opening parameter and 15 different values of the wall ruggedness parameter  $M_1$ , spanning the whole possible range  $[0, 98]$ . The fitted values of the normalised effective diffusion coefficient in the long-time regime,  $D_{\text{rel}}$ , are depicted in Fig. 6 as function of  $M_1$ . Here and in the following, solely the EATA MSD values were used, as they supply the most extensive data. The results obtained with the EA MSD data are very similar (data not shown), which is not surprising due to the ergodicity of the process at long times. In both cases, an increase of the wall ruggedness (larger  $M_1$  values) effects slower effective diffusion. The slope of this decrease is steepest for small  $M_1$  values and then gradually flattens off. Conversely, at fixed values of  $M_1$  the effective diffusion is always substantially faster for  $g = 6$  than  $g = 4$ .

To study the impact of the gap opening parameter  $g$  in more detail, we took five different values at fixed val-

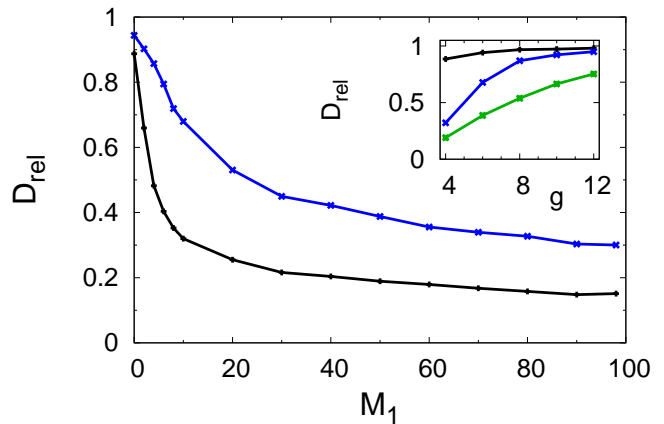


FIG. 6: Normalised effective long-time diffusion coefficient  $D_{\text{rel}}$  from fitting of the simulations results, as function of the wall ruggedness parameter  $M_1$ . Parameters: gap opening parameter  $g = 4$  (black symbols) and  $g = 6$  (blue symbols). Inset:  $D_{\text{rel}}$  as function of  $g$  for  $M_1 = 0$  (black symbols),  $M_1 = 10$  (blue symbols), and  $M_1 = 50$  (green symbols).

ues of the wall ruggedness parameter, namely,  $M_1 = 0$ ,  $M_1 = 10$ , and  $M_1 = 50$ . Thus, we consider flat channels, slightly corrugated, and heavily corrugated channels. The corresponding results for the fitted values of the normalised effective diffusion constant  $D_{\text{rel}}$  are shown in the inset of Fig. 6. For fixed value of  $g$  we see once more that the diffusion is quickest when the wall is smoother or, i.e., when  $M_1$  is smaller. As was already observed in the preceding paragraph a wider gap opening at a fixed value of  $M_1$  leads to faster diffusion. Thus, wider channels can be traversed quicker.

At first sight surprisingly, we observe that even for completely flat upper and lower channel walls ( $M_1 = 0$ , black line in the inset of Fig. 6) the diffusion in tighter channels is slowed down in comparison to the situation in free space. This is not expected in systems with reflecting boundaries, which are usually described with the Fick-Jacobs equation. However, for the finite-size particles studied here it is the result of the sticky boundary conditions at the channel walls: in a tighter channel the particle is more often close to the walls and binds transiently. Alternatively, the slow-down due to the interaction with the walls can be quantified by measuring the anomalous diffusion exponent  $\alpha$  in the intermediate time regime, on time scales  $10^3$  to  $10^5$  simulations steps. The fitted values for  $\alpha$  are depicted in Fig. 7 as function of the ruggedness  $M_1$ . The same trend as for the effective diffusion coefficient is seen for the anomalous diffusion exponent  $\alpha$  of the transient subdiffusive regime. For increasing contour lengths of the channel wall the motion is increasingly subdiffusive. As expected, the transient subdiffusion is heavier for the tighter channel ( $g = 4$ ).

The dependence of  $\alpha$  on the gap opening parameter is shown in the inset of Fig. 7. In this case, only values



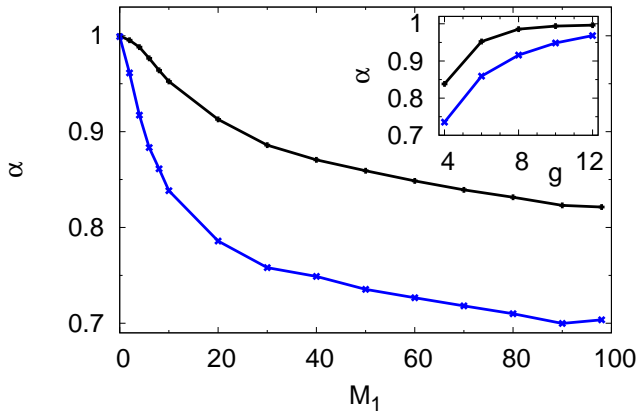


FIG. 7: Anomalous diffusion exponent  $\alpha$  as function of wall ruggedness  $M_1$  from power-law fit of the EATA MSD data. Parameters:  $g = 4$  (blue) and  $g = 6$  (black). Inset:  $\alpha$  as function of  $g$  for  $M_1 = 10$  (black), and  $M_1 = 50$  (blue).

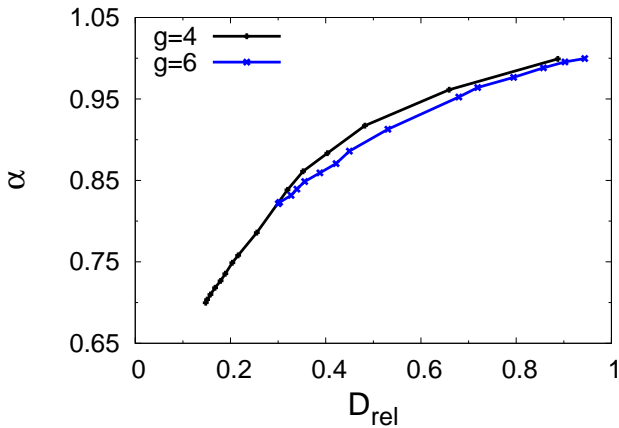


FIG. 8: Anomalous diffusion exponent  $\alpha$  of the transiently subdiffusive regime as function of the long-time diffusion exponent  $D_{\text{rel}}$  with gap opening parameters  $g = 4$  (black) and  $g = 6$  (blue).

obtained with corrugated channels ( $M_1 = 10$  and  $M_1 = 50$ ) are shown.[44] Again, the curves for  $\alpha$  are similar to the ones obtained for the effective diffusion coefficient:  $\alpha$  is an increasing function of  $g$  and  $M_1 = 10$  leads to less pronounced transient subdiffusion than  $M_1 = 50$ . This analogy motivates the study of the relation between  $\alpha$  and  $D_{\text{rel}}$  in more detail.

In Fig. 8 we plot all  $\alpha$  values for gap opening  $g = 4$  and  $g = 6$  as function of the corresponding fitted values of  $D_{\text{rel}}$ . The results show that there is a strong (nonlinear) correlation between both parameters. For increasing values of  $D_{\text{rel}}$  the value of  $\alpha$  also increases, with decreasing slope. The relation between both parameters is bijective, thus, both quantities are appropriate and sufficient to quantify the slow-down of the motion along the chan-

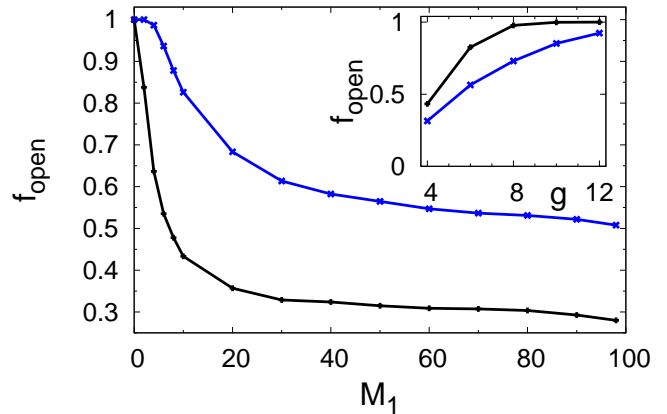


FIG. 9: Fraction  $f_{\text{open}}$  of unblocked configurations as function of the channel ruggedness  $M_1$  for channel opening  $g = 4$  (black) and  $g = 6$  (blue). Inset:  $f_{\text{open}}$  as function of  $g$  for  $M_1 = 10$  (black) and  $M_1 = 50$  (blue).

nel. For similar values of  $D_{\text{rel}}$  the values for  $\alpha$  obtained with the tighter channels ( $g = 4$ ) are slightly larger than those for the wider channels ( $g = 6$ ). However, this fact should not be overstated: all data sets were fitted in the time interval  $10^3$  to  $10^5$ , irrespective of the exact shapes of the curves. It is conceivable that a closer connection between the values for  $\alpha$  could have been obtained by choosing the fitting time window for each curve individually.

As mentioned above, in an ensemble of systems with corrugated boundaries not all channels can be traversed completely. If a channel is blocked somewhere, the corresponding squared displacement of the particle position has an upper limit. On an ensemble level these trajectories will reduce the average values of  $\alpha$  and  $D_{\text{rel}}$ . Thus, it is important to extract from our simulations solely the unblocked configurations. The corresponding parameter  $f_{\text{open}}$  is plotted as function of the ruggedness  $M_1$  for fixed gap openings  $g = 4$  (black symbols) and  $g = 6$  (blue symbols) in Fig. 9, and as function of the gap opening  $g$  (for  $M_1 = 10$  and  $M_1 = 50$ ) in the inset of Fig. 9. An inspection of Fig. 9 shows that this fraction is a decreasing function of  $M_1$  and an increasing function of  $g$ . Overall, the curves look similar to the ones of the normalised effective diffusion coefficient  $D_{\text{rel}}$  (compare Fig. 6).

To better understand why above a certain threshold of the boundary ruggedness parameter  $M_1$  the effective diffusion coefficient only decreases slightly (see Fig. 6), it is instructive to study the average weighted effective width  $w_{\text{wgt}}$  of the channels. Here, weighted means that for any blocked channel the width is set to zero. The weighted width is plotted as function of  $M_1$  in Fig. 10. For increasing, yet small values of  $M_1$  the effective weighted channel width decreases, until it reaches a shallow minimum beyond which  $w_{\text{wgt}}$  levels off to a plateau. While heavily rugged channel walls, in principle, can be tighter

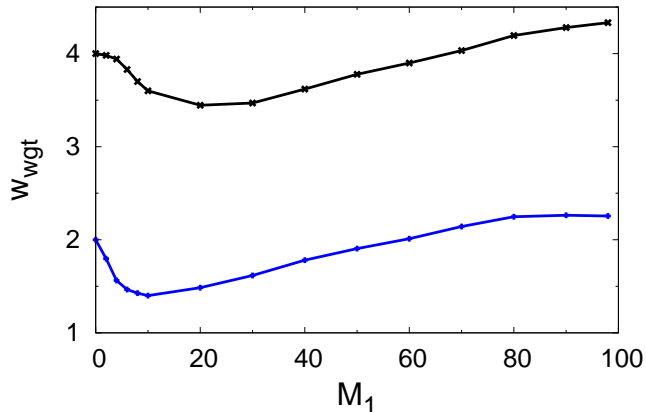


FIG. 10: Weighted effective channel width  $w_{\text{wgt}}$  as function of channel ruggedness  $M_1$  for gap opening  $g = 6$  (black line and symbols) and  $g = 4$  (blue line and symbols).

or more spacious than a flat configuration with the same gap opening  $g$ , the tighter ones are in constant ‘danger’ of precluding the particle passage. Thus, the average width of those traversable channels is larger for more rugged wall configurations. This facilitates the transport through these configurations, as the sticky boundaries are further away. However, as remarked earlier, more rugged walls slow down the diffusion due to the occurrence of bulges and constrictions [20], such that we have two opposing effects, which mostly (almost) cancel each other. Consequently,  $w_{\text{wgt}}$  (and thus  $D_{\text{rel}}$ ) reaches a plateau above a threshold value of  $M_1$ .

Fig. 11 shows the normalised effective diffusion coefficient  $D_{\text{rel}}$  as function of the weighted channel width  $w_{\text{wgt}}$ . For better visibility data points with identical  $M_1$  values are connected by lines ( $M_1 = 0$ : black line,  $M_1 = 10$ : blue line, and  $M_1 = 50$ : green line). While for a fixed value of  $M_1$  more spacious channels allow faster diffusion, the heavy scatter between values of  $D_{\text{rel}}$  obtained with similar values of  $w_{\text{wgt}}$  (grey symbols) shows that the knowledge of the mean channel width of an ensemble of channels alone is insufficient to predict the transport properties.

## V. COMPARISON WITH DAGDUG AND PINEDA’S FORMULA

In order to compare our results obtained from ensembles of channel configurations with the result of Dagdug and Pineda, we make a simplifying assumption: for all unblocked configurations, we determine  $D_{DP}(x)$  from Eq. 4 and subsequently  $D_{\text{eff,DP}}$  from Eq. 5. For all blocked configurations the effective diffusivity  $D_{\text{eff,DP}} = 0$  accounts for the fact that on long time-scales particles in these configurations do not contribute significantly to the MSD. Finally, we average over all configurations in

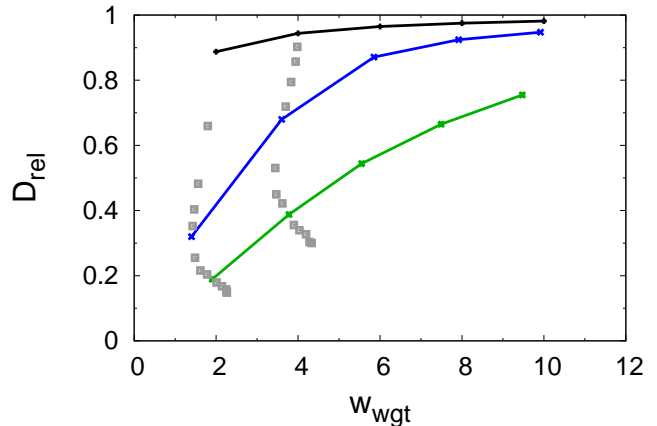


FIG. 11: Normalised effective diffusion coefficient  $D_{\text{rel}}$  as function of the weighted effective channel width  $w_{\text{wgt}}$  for  $M_1 = 0$  (black),  $M_1 = 10$  (blue line),  $M_1 = 50$  (green line) and other values of  $M_1$  (grey symbols).

the ensemble and normalise through division by the diffusion coefficient in free space,  $D_{\text{rel,DP}} = \langle D_{\text{eff,DP}} \rangle / D_0$ . We compare these values with our fitted values of the normalised diffusion coefficient in the upper panel of Fig. 12, where data points with the same value of the gap opening  $g$  are represented in the same colour.

This is the central result of our study: As demonstrated in the upper panel of Fig. 12, for fixed values of the gap opening  $g$  there is a linear relation between  $D_{\text{rel}}$  and  $D_{\text{rel,DP}}$ . Most of the data points are located within a 10% confidence interval around Dagdug and Pineda’s value. More explicitly, a linear fit of the data points obtained in a simulation series yields the following results. For  $g = 4$ , the fitted relation between the two is  $D_{\text{rel}} = (0.018 \pm 0.004) + (0.853 \pm 0.009)D_{\text{rel,DP}}$ , while for  $g = 6$  we find  $D_{\text{rel}} = (0.032 \pm 0.095) + (0.903 \pm 0.007)D_{\text{rel,DP}}$ . For  $g = 8, 10$ , and  $12$  we did not fit the data as there were only three values available.

The fact that the slope of the fits is somewhat below 1 shows that Dagdug and Pineda’s formula, which only applies to systems with perfectly reflecting boundaries slightly overestimates the diffusion coefficient compared to our system with sticky boundary conditions. Thus, as expected the additional interaction with the boundaries further slows down the diffusion, which is already reduced by the occurrence of entropic bottlenecks. This reasoning is further substantiated by the observation that in tighter channels (with  $g = 4$ ), where these surface effects play a more important role, the slope of the conversion formula is smaller, and the deviation from Dagdug and Pineda’s formula is more pronounced. Given the quite intricate form of the effective channel width (see Figs. 1 and 3) it is not feasible to quantify this effect analytically. However, in the future other values of  $s_1$  and  $s_2$  could be considered to study the magnitude of the correction terms numerically.



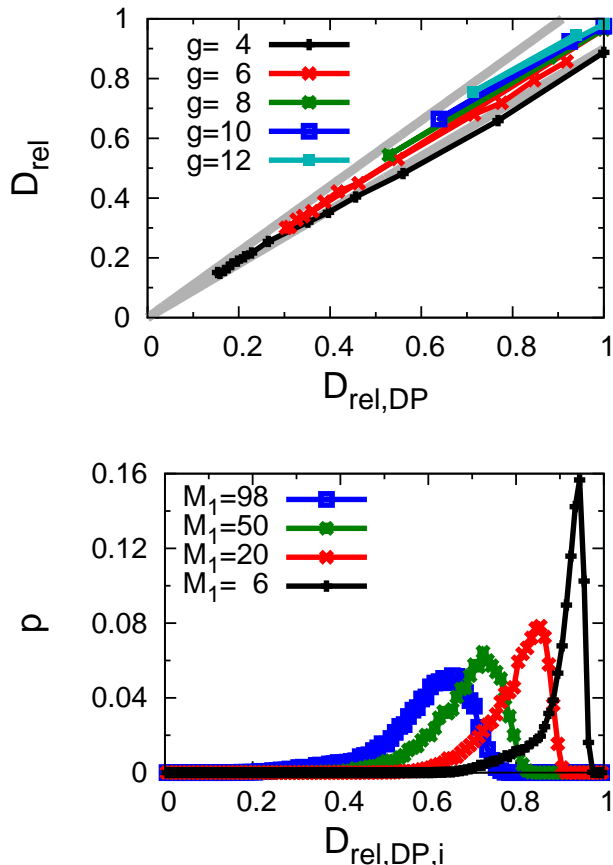


FIG. 12: Upper panel: normalised effective diffusion coefficient  $D_{\text{rel}}$  from our simulations in the sticky, corrugated channel as function of the value  $D_{\text{rel,DP}}$  obtained from the result (4) of Dagdug and Pineda. Black: gap opening parameter  $g = 4$ , red:  $g = 6$ , green:  $g = 8$ , blue:  $g = 10$ , and cyan:  $g = 12$ . The two grey lines mark the range of  $\pm 10\%$  around the theoretical value. Lower panel: distributions of effective diffusion coefficients for individual unblocked channel configurations obtained with Dagdug and Pineda’s formula. Parameters:  $g = 6$  in all four cases.  $M_1 = 6$ : black,  $M_1 = 20$ : red,  $M_1 = 50$ : green,  $M_1 = 98$ : blue.

That deviations of our results from Dagdug and Pineda’s formula are also based on the fact that their analysis applies to one given channel configuration. Driven by the physical application we here consider an ensemble of different channel wall configurations, solely defined by the fixed macroscopic parameters  $g$  and  $M_1$ . Individual configurations may therefore differ consider-

ably. This is illustrated in the lower panel of Fig. 12, where for all unblocked configurations the expected effective diffusion coefficient was calculated with Dagdug and Pineda’s formula. For  $g = 6$  and four different values of  $M_1$  we see that the distribution of values of  $D_{\text{rel,DP}}$  is far from narrow. The values increasingly scatter for more rugged conformations (higher values of  $M_1$ ). Thus, the semi-quantitative agreement of our data with the theoretical prediction on an ensemble level is indeed remarkable.

## VI. CONCLUSION AND OUTLOOK

We studied the motion of finite-size particles through randomly corrugated channels with sticky walls, observing transient anomalous diffusion of the particles in their passage of the channel. We also obtained the long-time diffusion coefficient for this motion on time scales over which normal Brownian diffusion is restored. The control parameters in our study were the gap opening parameter fixing the distance between the channel walls at the entrance and exit of the channel, as well as the wall ruggedness parameter setting the maximal variation of the channel wall configuration. We quantified the dependence of the anomalous diffusion exponent and long-time diffusion coefficient as function of the ruggedness and gap opening, and showed that both quantities are in fact correlated. We especially analysed the blocked channels, which the particle cannot fully traverse. The long-time effective diffusion coefficient was shown to agree well with the prediction for point-like particles in channels with reflecting boundary conditions by Dagdug and Pineda. Translated into the language of pathogens in hydrogels, whose motion we want to mimic in our numerical study of an ensemble of ‘parallel’ channels with identical gap opening and ruggedness, our study provides statistical information on how many channels are blocked for the pathogen passage.

In future studies it might be interesting to replace our minimal model of interactions with the constituents of the hydrogel with a more realistic model. In particular, the introduction of dynamic boundaries, for example by varying the gap opening during the simulations might be worth considering in order to model the structural change of the hydrogel due to the binding of pathogens.

MB and AG acknowledge funding from the German Federal Ministry for Education and research, and RM from the Academy of Finland within the FiDiPro scheme.

- 
- [1] D. Brockmann, L. Hufnagel, and T. Geisel, *Nature*, 2006, **439**, 462.  
 [2] K. E. Jones et al., *Nature*, 2008, **451**, 990.  
 [3] A. J. Alanis, *Arch. Med. Res.*, 2005, **36**, 697.  
 [4] R. S. Sellar and K. S. Peggs, *Brit. J. Haematol.*, 2012,

- 156**, 559.  
 [5] J. Holtz and S. Asher, *Nature*, 1997, **389**, 829.  
 [6] T. Miyata, N. Asami, and T. Uragami, *Nature*, 1999, **399**, 766.  
 [7] K. Gawel, D. Barriet, M. Sletmoen, and B. T. Stokke,

- Sensors*, 2010, **10**, 4381.
- [8] E. Wischerhoff, N. Badi, J.-F. Lutz, and A. Laschewsky, *Soft Matt.*, 2010, **6**, 705.
- [9] I. Y. Wong, M. L. Gardel, D. R. Reichman, E. R. Weeks, M. T. Valentine, A. R. Bausch, and D. A. Weitz, *Phys. Rev. Lett.*, 2004, **92**, 178101.
- [10] J.-H. Jeon, N. Leijnse, L. Oddershede, and R. Metzler, *New J. Phys.*, 2013, **15**, 045011.
- [11] G. Seisenberger, M. U. Ried, T. Endreß, H. Büning, M. Hallek and C. Bräuchle, *Science*, 2001, **294**, 1929.
- [12] J.-H. Jeon, V. Tejedor, S. Burov, E. Barkai, C. Selhuber-Unkel, K. Berg-Sørensen, L. Oddershede, and R. Metzler, *Phys. Rev. Lett.*, 2011, **106**, 048103.
- [13] S. M. A. Tabei, S. Burov, H. Y. Kim, A. Kuznetsov, T. Huynh, J. Jureller, L. H. Philipson, A. R. Dinner, and N. F. Scherer, *Proc. Natl. Acad. Sci. USA*, 2013, **110**, 4911.
- [14] R. Metzler and J. Klafter, *Phys. Rep.*, 2000, **339**, 1.
- [15] R. Metzler and J. Klafter, *J. Phys. A*, 2004, **37**, R161.
- [16] M. J. Saxton and K. Jacobson, *Ann. Rev. Biophys. Biomol. Struct.*, 1997, **26**, 373.
- [17] E. Barkai, Y. Garini, and R. Metzler, *Phys. Today*, 2012, **65**(8), 29.
- [18] F. Höfling and T. Franosch, *Rep. Prog. Phys.*, 2013, **76**, 046602.
- [19] P. S. Burada, P. Hänggi, F. Marchesoni, G. Schmid, and P. Talkner, *Chemphyschem*, 2009, **10**, 45.
- [20] R. Zwanzig, *J. Phys. Chem.*, 1992, **96**, 3926.
- [21] D. Reguera and J. M. Rubí, *Phys. Rev. E*, 2001, **64**, 061106.
- [22] P. Kalinay and J. K. Percus, *J. Chem. Phys.*, 2005, **122**, 204701.
- [23] P. Kalinay and J. K. Percus, *Phys. Rev. E*, 2005, **72**, 061203.
- [24] P. Kalinay and J. K. Percus, *Phys. Rev. E*, 2006, **74**, 041203.
- [25] A. M. Berezhkovskii, M. A. Pustovoit, and S. M. Bezrukov, *J. Chem. Phys.*, 2007, **126**, 134706.
- [26] P. Kalinay and J. K. Percus, *Phys. Rev. E*, 2008, **78**, 021103.
- [27] S. Martens, G. Schmid, L. Schimansky-Geier, and P. Hänggi, *Phys. Rev. E*, 2011, **83**, 051135.
- [28] A. Berezhkovskii and A. Szabo, *J. Chem. Phys.*, 2011, **135**, 074108.
- [29] P. Kalinay, *Phys. Rev. E*, 2013, **87**, 032143.
- [30] S. Martens, A. V. Straube, G. Schmid, L. Schimansky-Geier, and P. Hänggi, *Phys. Rev. Lett.*, 2013, **110**, 010601.
- [31] A. G. Cherstvy, A. V. Chechkin, and R. Metzler, *New J. Phys.*, 2013, **15**, 083039.
- [32] A. G. Cherstvy and R. Metzler, *Phys. Chem. Chem. Phys.*, 2013, **15**, 20220.
- [33] A. Fuliński, *Phys. Rev. E*, 2011, **83**, 061140.
- [34] A. Fuliński, *J. Chem. Phys.*, 2013, **138**, 021101.
- [35] R. M. Bradley, *Phys. Rev. E*, 2009, **80**, 061142.
- [36] L. Dagdug and I. Pineda, *J. Chem. Phys.*, 2012, **137**, 024107.
- [37] S. Lifson and J. L. Jackson, *J. Chem. Phys.*, 1962, **36**, 2410.
- [38] R. Festa and E. D'Agliano, *Physica A*, 1978, **90**, 229.
- [39] L. Dagdug, A. M. Berezhkovskii, Y. A. Makhnovskii, and V. Y. Zitserman, *J. Chem. Phys.*, 2008, **129**, 184706.
- [40] W. Riefler, G. Schmid, P. S. Burada and P. Hänggi, *J. Phys. Cond. Mat.*, 2010, **22**, 454109.
- [41] P. A. Netz and T. Dorfmueller, *J. Chem. Phys.*, 1995, **103**, 9074.
- [42] M. Saxton, *Biophys. J.*, 1996, **70**, 1250.
- [43] V. Tejedor, O. Bénichou, R. Voituriez, R. Jungmann, F. Simmel, C. Selhuber-Unkel, L. B. Oddershede, and R. Metzler, *Biophys. J.*, 2010, **98**, 1364.
- [44] In flat channels with  $M_1 = 0$  no transient subdiffusion occurs, see above.